NUCLEAR THEORY, Vol. 41 (2024)
eds. M. Gaidarov, N. Minkov, Heron Press, Sofia

Influence of Effective Surface Properties on Nuclear Structure within Coherent Density Fluctuation Model

Abdullah Modabbir[1], **Abdul Quddus**[2], **Shakeb Ahmad**[1,3]

[1]Department of Physics, Aligarh Muslim University, Aligarh-202002, India
[2]Applied Sciences and Humanities Section, University Polytechnic, Aligarh Muslim University, Aligarh – 202002, India
[3]Physics Section, Women's College, Aligarh Muslim University, Aligarh – 202002, India

Abstract. The equation of state of asymmetric nuclear matter is limited due to the undetermined symmetry energy and lack of initial constraint on the nuclear matter, leading to the evaluation of the nuclear matter symmetry energy with finite nuclei properties. The importance of symmetry energy and the tremendous possible features of $N = 40$ isotones have encouraged us to do a systematic study of effective surface properties of $N = 40$ isotonic series (from $Z = 18$ to $Z = 46$). The Coherent Density Fluctuation Model (CDFM) is used to estimate these surface properties in which densities of nuclei from relativistic mean field model are taken as the input. We have also calculated the bulk properties of the ground state, including pairing energy, binding energy, charge radii, single particle energy, and two proton separation energy. The calculated results are in good agreement with each other and also with the available experimental data. The effective surface properties show the change of their behavior at $Z = 20$, 28, and 40, which validates the shell closure properties/magic behavior of these proton numbers and support the same findings from the bulk properties. We have also witnessed that the skin thickness correlated with symmetry energy for the same isotonic series. The symmetry energy of N=40 is found to be correlated with nuclear structure properties. This study will help in the production of neutron-rich nuclei and also the constraints of heavy ion reactions.

1 Introduction

One of the main problems in nuclear physics is to constrain the equation of state (EOS) of nuclear matter (NM). It includes the basic characteristics of the nuclear systems, which are found in many astronomical objects and processes in addition to finite nuclei. Advancements in radioactive beam facilities and astrophysical observations can offer important constraints on the nuclear EOS. Density-dependent symmetry energy is one of the main parameters of EOS and has gained a lot of attention within the nuclear physics community. It is a crucial quantity in various aspects of nuclear physics, such as dynamics of heavy-ion

reactions [1–3], giant collective excitations [4], physics study of neutron stars [5–7], and ground state structure of nuclei [8–10]. Symmetry energy has a direct connection with the isospin asymmetry of the nuclear system, and it depends on the proton and neutron densities. Experimentally, the assessment of symmetry energy is not a directly accessible entity; its extraction is possible indirectly from one of the related observables like neutron skin-thickness. Another important determining quantity of EOS of nuclear matter is the slope parameter, which relates to the neutron pressure. Second-order derivative of symmetry energy is called as the symmetry energy curvature.

In the nuclear Segre chart, most of the stable nuclei are found to be around β-stability line; the nuclei with the large neutron-to-proton ratio (drip-line nuclei) are currently an interesting subject to study. A number of experiments are being conducted to investigate exotic nuclear systems (finite) under the utmost isospin asymmetry conditions with the advancements in radioactive beam facilities. In addition to a wide range of previously unknown exotic behavior, one of the most intriguing ones is the emergence of contemporary magic numbers in the drip-line area of the nuclear chart. Moreover, the deformed ground states of nuclei with a large N/Z ratio and new evidence for the possible existence of an "island of inversion" make it fascinating [11] to examine the drip-line nuclei. Therefore, exploring the structure of drip-line nuclei with a method based mostly on isospin asymmetry and neutron-proton chemical potentials will be of great interest. Nuclear matter with asymmetry of proton and neutron and astrophysical systems, notably neutron stars, can be linked with a nucleus isospin asymmetry, especially if it is far from the stability line.

At the University of Tokyo, RIKEN laboratory, Nishina Center and CNS discovered the $^{60}_{20}\mathrm{Ca}_{40}$ [12], which has raised an interest in exploring the theoretical and experimental aspects of nuclei consisting of $N = 40$ isotones. For the $N = 40$ isotones toward ^{60}Ca [13], a detailed analysis of shell evolution has been reported after the first spectroscopy of ^{62}Ti. $^{68}_{28}\mathrm{Ni}_{40}$ is another nucleus that has demonstrated enormous possibilities for studying magicity [14] and shape coexistence [15] around $Z = 40$. In Ref. [16], a study was done for the N=40 isotones using the covariant density functional theory, that provides the shape-mixing of N=40 isotones along with the coexistence of low-lying excited of 0^+ state in the neutron deficient region. Along with the recent experimental findings, evidence of new island of inversion near $N(Z) = 40$ [17, 18] with waiting point nuclei along the $N = Z$ line being pivotal in rapid proton capture reactions (rp-process) [19], tell the importance of nuclei around $N(Z) = 40$. Therefore, the importance of density-dependent symmetry energy and the tremendous possible features of $N = 40$ isotones have encouraged us to do a systematic study of symmetry energy, neutron pressure, and symmetry energy curvature to see their influence on nuclear structure. The densities used in calculating the surface properties are obtained from the relativistic mean field (RMF) model [20, 21]; along with the bulk properties of the nuclei. We have used the coherent density fluctuation model (CDFM) to evaluate the symmetry energy, neutron pres-

sure, and symmetry energy curvature, collectively known as the effective surface properties.

The following is the format of the paper: The formalism of the work is contained in Section 2. We introduce the RMF in Section 2.1 in order to acquire the densities and the properties of nuclei. The importance parameters of EOS of nuclear matter are described in Section 2.2. The CDFM for determining finite nuclei's surface attributes is presented in Section 2.3. The findings and potential linkages were covered in Section 3. The conclusion of the findings is provided in Section 4.

2 Formalism

2.1 Relativistic Mean-Field theory (RMF)

Following multiple modifications to the original Walecka Lagrangian [23, 24] to address various limitations, a standard relativistic Lagrangian density with the self coupling of the ω_μ field and the cross coupling of ω_μ and $\vec{\rho_\mu}$ fields for a hadron-meson many-body nuclear system adopts the following form [21,25–28].

$$\begin{aligned}\mathcal{L}(r_\perp, z) =& \bar{\psi}(r_\perp, z)(i\gamma^\mu\partial_\mu - M + g_s\sigma - g_\omega\gamma^\mu\omega_\mu - g_\mu\gamma^\mu\tau\vec{\rho_\mu} \\ & - e\gamma^\mu\frac{1+\tau_3}{2}A_\mu)\psi(r_\perp, z) + \frac{1}{2}(\partial_\mu\partial^\mu - m_\sigma^2\sigma^2) - \frac{1}{4}\Omega^{\mu\nu}\Omega_{\mu\nu} \\ & + \frac{1}{2}m_\omega^2\omega_\mu\omega^\mu - \frac{1}{4}\vec{R}^{\mu\nu}\vec{R}_{\mu\nu} + \frac{1}{2}m_\rho^2\vec{\rho_\mu}\vec{\rho^\mu} - \frac{1}{4}F^{\mu\nu}F_{\mu\nu} \\ & - m_s^2\sigma^2\left(\frac{k_3}{3!}\frac{g_s\sigma}{3} + \frac{k_4}{4!}\frac{g_s^2\sigma^2}{M^2}\right) + \frac{1}{4!}\zeta_0 g_\omega^2(\omega^\mu\omega_\mu)^2 \\ & + \Lambda_\omega g_\omega^2 g_\rho^2\omega^\mu\omega_\mu(\vec{\rho^\mu}\vec{\rho_\mu}) \end{aligned} \tag{1}$$

with vector field tensors:

$$\Omega^{\mu\nu} = \partial^\mu\omega^\nu - \partial^\nu\omega^\mu\,, \tag{2}$$

$$\vec{R}^{\mu\nu} = \partial^\mu\vec{\rho}^\nu - \partial^\nu\vec{\rho}^\mu\,, \tag{3}$$

$$F^{\mu\nu} = \partial^\mu A^\nu - \partial^\mu A^\nu\,, \tag{4}$$

where σ, ω_μ, $\vec{\rho}_\mu$ are the fields for the σ-, ω-, ρ-mesons and A_μ is the electromagnetic field with respective coupling constants g_σ, g_ω, g_ρ, $e^2/4\pi$. Masses for σ-, ω-, ρ-mesons are, respectively, m_σ, m_ω, m_ρ.

We have used this Lagrangian density to find the bulk properties of the nuclei, including the density distribution, using two sets of non-linear parameters, NL3 [21] and IOPB-I [29]. A constant-gap BCS approach [21–23] has been employed for the open-shell nuclei.

2.2 Nuclear matter properties

Energy density $\mathcal{E}(\rho,\alpha)$ is expanded through the Taylor series expansion in terms of the asymmetry coefficient $\alpha = (\rho_n - \rho_p)/(\rho_n + \rho_p)$:

$$\mathcal{E}(\rho,\alpha) = \mathcal{E}(\rho) + C(\rho)\alpha^2 + O(\alpha^4)\,. \tag{5}$$

Here, $\mathcal{E}(\rho)$, $C(\rho)$ are the symmetric nuclear matter ($\alpha = 0$) energy density and symmetry energy as a function of baryonic density (ρ), respectively. Notably, the isospin symmetry prohibits the odd powers of α, and the higher-order terms, including α^4, have a small impact. From the above expression, symmetry energy of nuclear matter $C(\rho)$ can be evaluated as

$$C(\rho) = \frac{1}{2}\left[\frac{\partial^2\mathcal{E}(\rho,\alpha)}{\partial\alpha^2}\right]_{\alpha=0}\,. \tag{6}$$

The Taylor series expansion approach can further be employed to expand the symmetry energy near the saturation density ρ_0. The expanded expression is

$$C(\rho) = J + L\zeta + \frac{1}{2}K\zeta^2 + \frac{1}{6}Q\zeta^3 + \cdots\,. \tag{7}$$

Here, $\zeta = (\rho - \rho_0)/3\rho_0$, and J is the symmetry energy at saturation density $C(\rho_0)$. The coefficient of ζ in the above equation is the slope parameter $L = 3\rho_0\left(\dfrac{\partial C(\rho)}{\partial\rho}\right)_{\rho_0} = 3\left(\dfrac{P_0}{\rho}\right)_{\rho_0}$ where P_0 is the neutron pressure of asymmetrical nuclear matter, and K is the symmetry energy curvature of nuclear matter. Further, the symmetry energy, neutron pressure, and symmetry energy curvature at the local density of finite nuclei are evaluated by using the Coherent Density Fluctuation Model.

2.3 Coherent Density Fluctuation Model (CDFM)

In the CDFM [30, 31], one-body density matrix $\rho(\boldsymbol{r},\boldsymbol{r'})$ of a nucleus can be expressed as a coherent superposition of an infinite number of one-body density matrices $\rho_x(\boldsymbol{r},\boldsymbol{r'})$ for a spherical "pieces" of nuclear matter called *fluctons* with densities.

$$i\rho_x(\boldsymbol{r},\boldsymbol{r'}) = \rho_0(x)\Theta(x - |\boldsymbol{r}|)\,, \qquad \rho_0(x) = \frac{3A}{4\pi x^3}\,. \tag{8}$$

The spherical radius of the nucleus contained in a uniformly distributed spherical Fermi gas is referred as the generator coordinate (x). The one-body density matrix in a finite nuclear system can be expressed as:

$$\rho(\boldsymbol{r},\boldsymbol{r'}) = \int_0^\infty dx|F(x)|^2\rho_x(\boldsymbol{r},\boldsymbol{r'})\,, \tag{9}$$

where $|F(x)|^2$ is the weight function defined in equation (12). The coherent superposition of the one-body density matrix is represented by the expression $\rho_x(\boldsymbol{r}, \boldsymbol{r'})$ [25, 30]. The one-body density matrix's Wigner distribution function can be expressed as follows:

$$W(\boldsymbol{r}, \boldsymbol{k}) = \int_0^\infty dx |F(x)|^2 W_x(\boldsymbol{r}, \boldsymbol{k}) \,, \tag{10}$$

where $W_x(\boldsymbol{r}, \boldsymbol{k}) = 4/(2\pi)^2 \Theta(x - |\boldsymbol{r}|)\Theta(k_f(x) - |\boldsymbol{k}|)$ and $k_f(x)$ is the Fermi momentum at local coordinate. In a similar way, the same weight function $|F(x)|^2$ is utilized to express the density $\rho(\boldsymbol{r})$ in the CDFM.

$$\begin{aligned} \rho(\boldsymbol{r}) &= \int d\boldsymbol{k} W(\boldsymbol{r}, \boldsymbol{k}) \\ &= \int_0^\infty dx |F(x)|^2 \frac{3A}{4\pi x^3} \Theta(x - |\boldsymbol{r}|) \,. \end{aligned} \tag{11}$$

The density $\rho(r)$ in the above equation is normalized to nucleon number A as $\int \rho(\boldsymbol{r}) d\boldsymbol{r} = A$. The differential equation for the weight function in the generator coordinate can be derived using the δ-function approximation of the Hill-Wheeler integral equation. For a given density distribution $\rho(r)$, the weight function is given by:

$$|F(x)|^2 = -\left(\frac{1}{\rho_0(x)} \frac{d\rho(r)}{dr} \right)_{r=x} \tag{12}$$

with $\int_0^\infty dx |F(x)|^2 = 1$

The properties of finite nuclei, such as symmetry energy S, neutron pressure P and symmetry energy curvature K_{sym} can be found from the infinite nuclear matter properties by folding them with the weight function $|F(x)|^2$

$$S = \int_0^\infty dx |F(x)|^2 C(\rho) \,, \tag{13}$$

$$P = \int_0^\infty dx |F(x)|^2 P_0(\rho) \,, \tag{14}$$

$$K_{\text{sym}} = \int_0^\infty dx |F(x)|^2 K(\rho) \,. \tag{15}$$

3 Results and Discussions

The current study examines nuclear symmetry energy, neutron pressure, and symmetry energy curvature for the isotonic series of $N = 40$. The self-consistent axially deformed RMF model is used to calculate the bulk properties, including pairing energy, binding energy per nucleon, and charge radii with commonly used NL3 [21] and recently generated IOPB-I [29] force parameters.

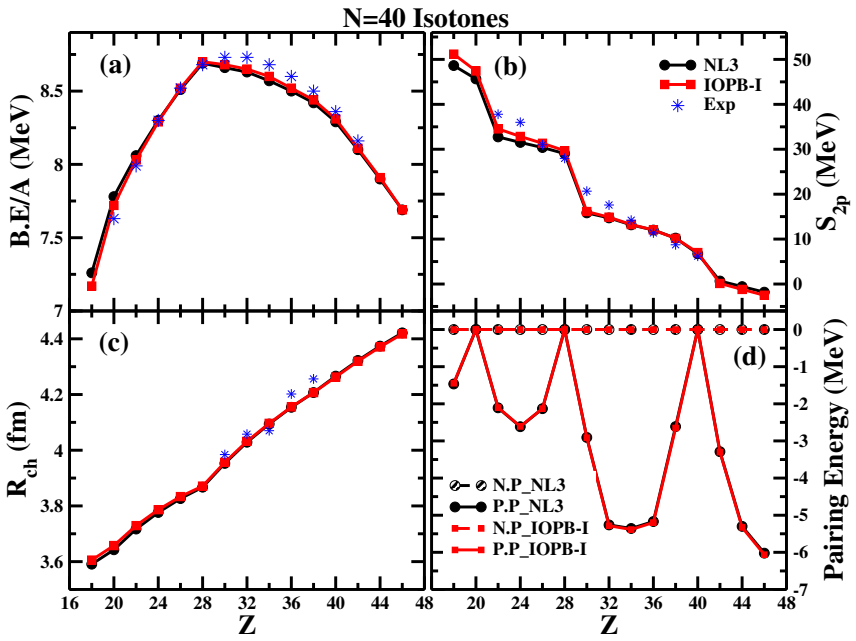

Figure 1. Shows binding energy per nucleon (a), charge radius (b), and pairing energy (c) with proton number Z for the NL3 (black) and IOPB-I(red) parameters sets of $N = 40$ isotonic series.

Panels (a) and (b) of Figure 1 show the variation of binding energy per nucleon (B.E/A) and two proton separation energy (S_{2p}), respectively, with atomic number Z. The results corresponding to NL3 and IOPB-I forces are represented by black and red curves, respectively, as the legends exhibit. And, this representation is kept same throughout the work. The results corresponding to both of the interactions are in agreement with each other and also with the available experimental results [32] (represented by star). There are some changes in the slope of the curves (or, kinks) at $Z = 20$, 28, and 40. The former two values of Z are standard proton magic numbers and the later is the predicted one. Panel (c) of the figure exhibits the charge radii $R_{\rm ch}$ that has less values corresponding to these magic numbers. In panel (d), neutron and proton pairing energies are plotted. The nuclei corresponding to the aforementioned proton numbers have zero proton pairing energy which signifies that these nuclei are more stable as compared to the surrounding ones. The pairing energy curves reproduce the shell closure nature of $Z = 20$ and 28, and support the sub-shell closure of $Z = 40$ as predicted in panels (a) and (b). Over the whole isotonic series the neutron pairing energy is found to be zero, which means the nucleons are fully paired in the corresponding energy level.

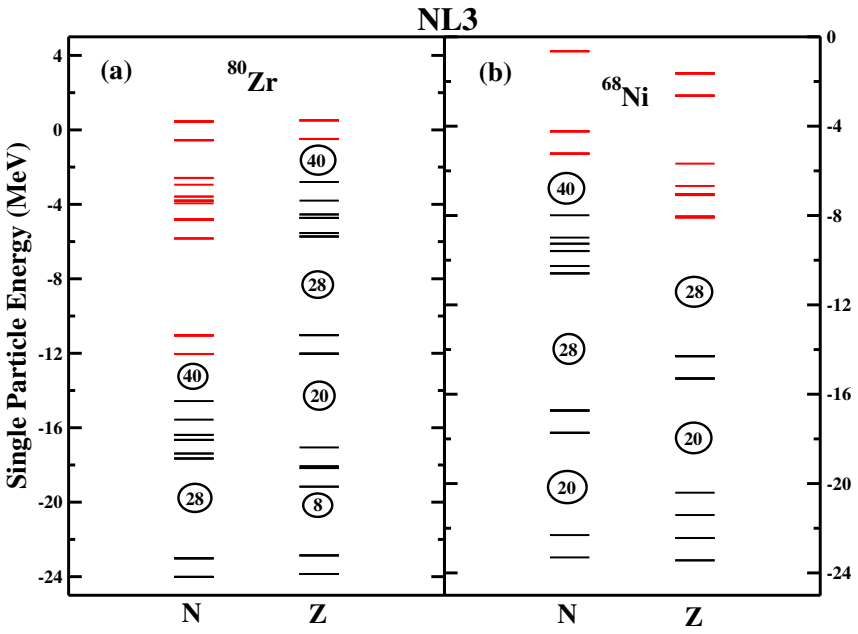

Figure 2. Single particle energy of ^{80}Zr (a) and ^{68}Ni (b) as representative case.

Another important property of a nucleus to confirm the shell/sub-shell closure nature is the single particle energy (SPE), which is shown in Figure 2. We have shown the neutron and proton single particle energies of ^{80}Zr and ^{68}Ni as a representative cases in panels (a) and (b), respectively. From the plot, it is clear that the difference between the energy levels at neutron(proton) magic number $N(Z) = 20$, 28 and 40 is greater compared to the other energy levels. This finding support the remarks made on Figure 1 and also in a good agreement with the work of Ref. [33].

The S, P, and K_{sym} for the $N = 40$ isotonic chain are presented in Figure 3 in the panels marked therein. Based on the figures, one can conclude that for isotonic chains, the variation of the S, P, and K_{sym} increase linearly up to $Z = 28$. Beyond this point, all these quantities gradually decrease with some change in the slopes at $Z = 40$. This changing slope point is in accord with the ground-state properties and can be inferred as the semi-magic number. Additionally, the isotonic chain exhibits kinks in the curves caused by the nuclei with double-shell closures at $Z = 20$, 28. From the same plot, one can see that the nature of symmetry energy and neutron pressure are reciprocal to each other, with NL3 as the stiffer EOS and IOPB-I as the softer EOS. The weight function has a significant values in the outer region of density distribution (not shown here) where density is lower than the saturation point density, and it is remarked in [34]

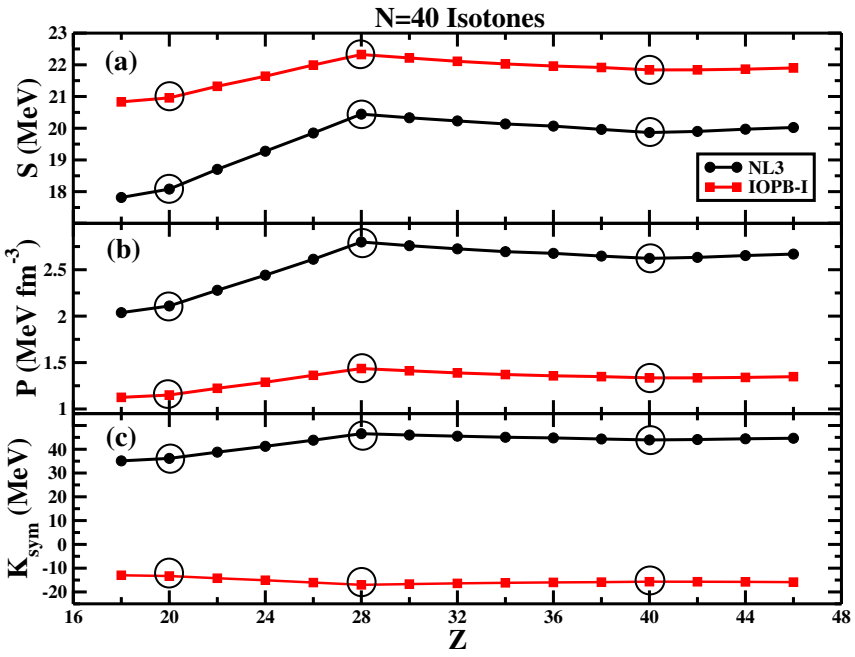

Figure 3. Variation of symmetry energy (a), neutron pressure (b), and symmetry energy curvature (c) with proton number Z for the NL3 (black) and IOPB-I(red) parameters sets of $N = 40$ isotonic series.

that below the saturation point, the value of S for NL3 is lower than that of the IOPB-I parameter.

Figure 4 shows the correlation of effective surface properties of the isotonic series with neutron skin-thickness Δr. From the figure, one can see a smooth trend of the symmetry energy, neutron pressure, and symmetry energy curvature with the neutron skin-thickness. In these curves also, there are some kinks or change of trends at $Z = 20$, 28 and 40, which correspond to double shell-closure/magic number. Neutron skin-thickness Δr of the black line (NL3) is found to be larger than the solid red line (IOPB-I). This is because the NL3 is a stiffer equation of state while IOPB-I is a softer equation of state. Since the symmetry energy is not a directly measurable quantity, it can be extracted from the indirect/ related quantities, one of which is neutron skin thickness.

4 Conclusion

In this work, we estimated the effective surface properties of N=40 isotonic chain, and their correlation with Δr using the CDFM. The bulk properties such as binding energy per nucleon, two proton separation energy, charge radii, pairing energy, and SPE of the $N = 40$ isotones are studied within the axially

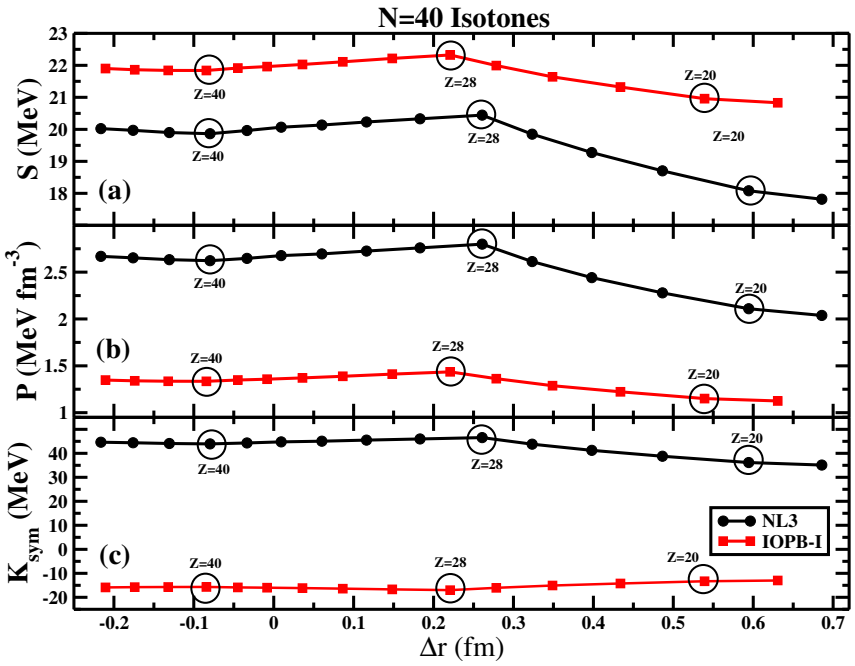

Figure 4. Correlation curves of neutron skin-thickness Δr with the Symmetry energy (a), neutron pressure (b), and symmetry energy curvature (c) for the NL3 (black) and IOPB-I (red) parameters sets.

deformed RMF with two sets of force parameters NL3, and IOPB-I. A good agreement of these results is seen with each other and also with the available experimental data. The estimated results reproduce the standard proton magic numbers $Z = 20$, and 28 and predict one more at $Z = 40$. The densities obtained from the RMF formalism are used in the CDFM to estimate the effective surface properties of the isotonic series.

The neutron skin-thickness of NL3 is found to be larger than that of the IOPB-I due to stiffer nature of EOS. The behavior of curves of effective surface properties represent the magicity at standard and predicted proton magic numbers. The $Z = 40$ as a magic is not only predicted by the ground state bulk properties, but also supported by the nature of the surface properties. This study will further help us to constrain the equation of state since the initial constraints are few, as well as in the production of neutron-rich nuclei.

Acknowledgements

A. Modabbir would like to acknowledge the NBCFDC, Govt. of India, for providing financial support through an NFOBC fellowship with No.202324-231620094281.

References

[1] B.-A. Li, L.-W. Chen, C.M. Ko, *Phys. Rep.* **464** (2008) 113.

[2] L.-W. Chen, C.M. Ko, B.-A. Li, G.-C. Yong, *Int. J. Mod. Phys. E* **17** (2008) 1825.

[3] M. Colonna, *J. Phys. Conf. Ser.* **168** (2009) 012006.

[4] V. Rodin, *Prog. Part. Nucl. Phys.* **59** (2007) 268.

[5] A.W. Steiner, M. Prakash, J.M. Lattimer, P.J. Ellis, *Phys. Rep. 411* (2005) 325.

[6] V.P. Psonis, Ch.C. Moustakidis, S.E. Massen, *Mod. Phys. Lett. A* **22** (2007) 1233 (2007).

[7] B.K. Sharma, S. Pal, *Phys. Lett. B* **682** (2009) 23.

[8] T. Nikšić, D. Vretenar, P. Ring, *Phys. Rev. C* **78** (2008) 034318.

[9] N. Van Giai, B.V. Carlson, Z. Ma, H. Wolter, *J. Phys. G* **37** (2010) 064043.

[10] E.N.E. van Dalen, H. Müther, *Int. J. Mod. Phys.* **19** (2010) 2077.

[11] C. Santamaria, C. Louchart, A. Obertelli, et al., *Phys. Rev. Lett.* **115** (2015) 192501.

[12] O.B. Tarasov, et al., *Phys. Rev. Lett.* **121** (2018) 022501.

[13] M.L. Cortés, et al., *Phys. Lett. B* **800** (2020) 135071.

[14] C. Izzo, et al., *Phys. Rev. C* **97** (2018) 014309.

[15] F. Flavigny, et al., *Phys. Rev. C* **99** (2019) 054332.

[16] Z.H. Wang, J. Xiang, W.H. Long, Z.P. Li, *J. Phys. G: Nucl. Part. Phys.* **42** (2015) 045108.

[17] P. Adrich, et al., *Phys. Rev. C* **77** (2008) 054306.

[18] S. Naimi, et al., *Phys. Rev. C* **86** (2012) 014325.

[19] B.A. Brown, R.R.C. Clement, H. Schatz, A. Volya, W.A. Richter, *Phys. Rev. C* **65** (2002) 045802.

[20] M. Dutra, O. Loureno, S.S. Avancini, et al., *Phys. Rev. C* **90** (2014) 055203.

[21] G.A. Lalazissis, S. Karatzikos, R. Fossion, D.P. Arteaga, A.V. Afanasjev, P. Ring, *Phys. Lett. B* **36** (2009) 671.

[22] S.K. Patra, M. Bhuyan, M.S. Mehta, R.K. Gupta, *Phys. Rev. C* **80** (2009) 034312.

[23] B.B. Serot, J.D. Walecka, *Adv. Nucl. Phys.* **16** (1986) 1.

[24] J.D. Walecka, *Ann. Phys., NY* **83** (1974) 491.

[25] M. Bhuyan, B.V. Carlson, S.K. Patra, S.G. Zhou, *Phys. Rev. C* **97** (2018) 024322.

[26] J. Boguta, A.R. Bodmer, *Nucl. Phys. A* **292** (1977) 413.

[27] B.V. Carlson, D. Hirata, *Phys. Rev. C* **65** (2000) 054310.

[28] T. Nikšić, D. Vretenar, P. Finelli, P. Ring, *Phys. Rev. C* **66** (2002) 024306.

[29] B. Kumar, S.K. Patra, B.K. Agrawal, *Phys. Rev. C* **97** (2018) 045806.

[30] A.N. Antonov, V.A. Nikolaev, I.Zh. Petkov, *Bulg. J. Phys.* **6** (1979) 151; *Z. Phys. A* **297** (1980) 257; **304** (1982) 239; *Nuovo Cimento A* **86** (1085) 23; A.N. Antonov, et al., ibid. **102** (1989) 1701.

[31] A.N. Antonov, D.N. Kadrev, P.E. Hodgson, *Phys. Rev. C 50* (1994) 164.

[32] National Nuclear Data Center, www.nndc.bnl.gov.

[33] R. Sharma, A. Jain, M. Kaushik, S.K. Jain, G. Saxena, *Int. J. Mod. Phys. E* **30** (2021) 2150070.

[34] Abdul Quddus, M. Bhuyan, Shakeb Ahmad, B.V. Carlson, S.K. Patra, *Phys. Rev. C* **99** (2019) 044314.